ACCUMULATOR RING DESIGN FOR THE EUROPEAN SPALLATION SOURCE NEUTRINO SUPER BEAM

JAKOB JONNERBY

Degree project C in Physics, 15 hp

Bachelor programme in Physics
Division of High Energy Physics
Department of Physics and Astronomy
Uppsala University

SUPERVISOR: Elena Wildner, CERN
SUBJECT READER: Tord Ekelöf, Uppsala University
EXAMINATOR: Susanne Mirbt, Uppsala University

June 2014

Jakob Jonnerby: *Accumulator Ring Design for the European Spallation Source Neutrino Super Beam,* Degree project C in Physics, 15 hp, © June 2014

LOCATION:
CERN, Geneva

June 2014

ABSTRACT

In this thesis, the design of a high intensity accumulator ring for the European Spallation Source Neutrino Super Beam (ESSnuSB) is considered. The European Spallation Source (ESS) linear accelerator (Linac), presently being constructed in Lund, Sweden, presents an interesting opportunity to also host an experiment to detect neutrino CP violation. 0.7 ms long H^-pulses would be accelerated to 2 GeV and collide with a target, producing pions which then decay into neutrinos. To focus the pions a toroidal magnet (”neutrino horn”) is pulsed with a 350 kA current. The peak current is about 5 μs long, which requires the H^-pulses to be shortened to about the same length using an accumulator ring that is located between the linac and the target. The H^-would be stripped of their electrons using either a thin carbon foil or a laser beam during injection into the ring. Foil stripping is limited by the lifetime of the foil, which depends on the temperature to which it is heated by the beam. The temperature is simulated in a computer model and the results indicate that it does not rise above the critical temperature (2500 K). The high number of protons (10^{15}) circulating in the ring could cause instabilities due to the collective charge of the particles, known as the space charge effect. The space charge tune shift is calculated for the ESSnuSB and different solutions are discussed. The result of a design accumulator lattice for the ESSnuSB, based on the Spallation Neutron Source, at Oak Ridge National Laboratory, Tennessee, U.S., and made using the computer program Methodical Accelerator Design (MAD), is presented.

SAMMANFATTNING

I den här uppsatsen behandlas designen av en högintensiv ackumulatorring för European Spallation Source Neutrino Super Beam (ESSnuSB). European Spallation Source (ESS) linjäraccelerator (linac), under konstruktion utanför Lund, Sverige, erbjuder en intressant möjlighet att också användas i ett experiment för att detektera CP-brott hos neutriner. 0.7 ms långa H^--pulser acceleras till 2 GeV och kolliderar med ett mål för att producera pioner, vilka senare sönderfaller till neutriner. För att fokusera pionerna så pulseras en magnet med en ström på 350 kA. Toppen på pulsen är cirka 5 μs lång, vilket medför att H^--pulserna måste kortas ned till samma längd med en ackumulatorring, placerad mellan linacen och målstationen. Elektronerna avlÃ€gsnas frÃ¥n H^--strålen under injektionen in i ringen genom att använda antingen en tunn kolfolie eller en laserstråle. Kolfoliemetoden begränsas av foliens livstid, vilken beror på temperaturen som den upphettas till av den infallande strålen. Temperaturen har simulerats i en datormodell och resultaten tyder på att den inte stiger ovanför den kritiska temperaturen (2500 K). Det höga antalet protoner (10^{15}) som cirkulerar i ringen kan medföra instabiliteter på grund av partiklarnas totala laddning, så kallad rymdladdning. Tonskiftet på grund av rymdladdningen har beräknats för ESSnuSB och olika lösningar har diskuterats. En stråloptikdesign för ackumulatorringen, baserat på Spallation Neutron Source vid det nationella laboratoriet i Oak Ridge, Tennessee, USA, har designats i datorprogrammet Methodical Accelerator Design (MAD).

CONTENTS

1

THE ESSNUSB PROJECT

1.1 BACKGROUND

Neutrinos are neutral, weakly interacting particles of small mass that come in three flavors: electron, muon, and tau neutrinos. These flavours were previously thought to be conserved, e.g. that a neutrino produced as an electron neutrino would remain an electron neutrino. However, the so-called *solar neutrino problem* (see [1]), called for a new model where the neutrino mass eigenstates ν_1, ν_2 and ν_3 are described as a superposition of the flavor eigenstates ν_e, ν_μ and ν_τ. The relative amount of each type of flavor eigenstate in each mass eigenstate are given by the mixing angles θ_{13}, θ_{23}, and θ_{12}. $\theta_{13}$was the last of the mixing angles to be measured, in 2012, and it turned out to be unexpectedly high [2].

MIXING ANGLE	VALUE	SOURCE
θ_{13}	8.83°	[2]
θ_{23}	45°	[3]
θ_{12}	34°	[3]

Table 1: Neutrino mixing angles

It remains an open question whether neutrinos violate Charge-Parity (CP) symmetry. If neutrinos and antineutrions behave differently in an oscillation experiment it would be an indication of CP-violation [1], and to discover it would be of fundamental importance for our understanding of cosmology. In the Big Bang, matter and antimatter was created in equal amounts. All of the antimatter was annihilated, but a fraction of the matter survived to make up of all of the visible universe today. Neutrinos could provide an explanation through a process called *leptogenesis*, in which neutrinos are thought to have heavy partner particles that decay into leptons and quarks, which makes up visible matter. If neutrinos violate CP, their heavy partners could decay into matter and antimatter with slightly different probabilities, explaining the dominance of matter over antimatter in the universe [4].

To measure CP-violation, the oscillation between muon and electron neutrinos are studied. The probability of oscillation from a muon neutrino into an electron neutrino can be approximated as [5]:

$$P^{\pm}_{\mu e} = s^2_{23} \sin^2 2\theta_{13} \sin^2\left(\frac{\Delta_{31}L}{2}\right) \tag{1}$$

$$+ c^2_{23} \sin^2 2\theta_{12} \sin^2\left(\frac{\Delta_{21}L}{2}\right) \tag{2}$$

$$+ \tilde{J} \cos\left(\pm\delta - \frac{\Delta_{31}L}{2}\right) \cdot \sin\left(\frac{\Delta_{21}L}{2}\right) \sin\left(\frac{\Delta_{31}L}{2}\right), \tag{3}$$

where the $+,-$ refers to neutrinos and antineutrinos, respectively, $\tilde{J} = c_{13} \sin 2\theta_{12} \sin 2\theta_{23} \sin 2\theta_{13}$, and $\Delta_{ij} = \delta m^2_{ij}/2E_\nu$. (1), (2), and (3) are called atmospheric, solar, and CP interference terms, respectively. Neutrino CP-violation is caused by the δ term in (3). In figure 1.2 these terms are plotted as a function of L/E (km/GeV) for low (1°) and high (10°) values of θ_{13} respectively. The high value of θ_{13} has opened up the possibility of a neutrino oscillation experiment with a detector at the second oscillation maximum rather than, as previosly planned, at the first maximum.

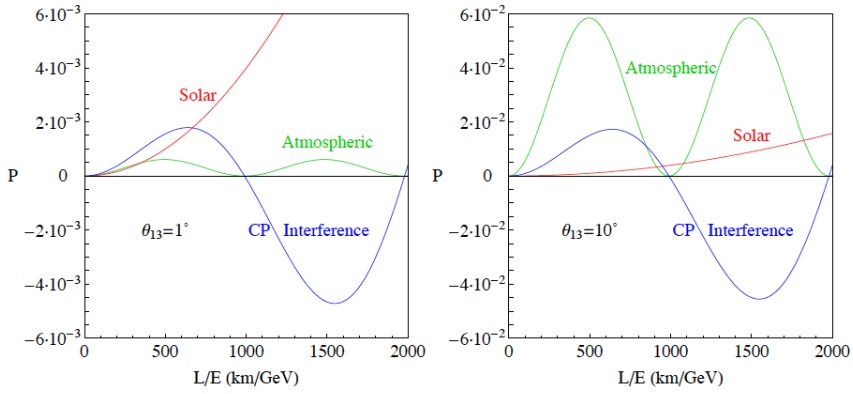

Figure 1.1: Neutrino oscillation probabilities for low (left) and high (right) values of θ_{13}. For a high θ_{13} the CP interference term is biggest at the second oscillation peak, compared with the atmospheric and solar oscillation terms. This is gives the optimal baseline length/energy ratio L/E for a neutrino oscillation of the type $\nu_\mu \rightarrow \nu_e$[5].

The European Spallation Source Neutrino Super Beam (ESSnuSB) is a proposed long baseline neutrino experiment to detect and measure neutrino CP violation using the high-intensity proton beam in the European Spallation Source (ESS). ESS is a neutron spallation source for material research to be constructed outside Lund, Sweden, and it will use the most intense proton linac in the world - accelerating 1.1×10^{15} protons to 2 GeV. If the ESSnuSB project is accepted, the ESS linac will be upgraded to 70 Hz to also accelerate H^-pulses between the proton pulses. The neutrinos will be produced by colliding

the intense beam with a titanium target. A 500 kton water Cherenkov detector located near the second oscillation maximum will count the number of muon neutrinos that oscillate to electron neutrinos. If neutrinos and antineutrinos oscillate at different rates, this would be an indication of CP-violation.

1.2 THE ESS LINEAR ACCELERATOR

In the ESS linac, the protons are produced in a source and accelerated to 2 GeV kinetic energy [6]. The H^- pulses needed for the ESSnuSB experiment would be produced in a separate source. The linac would be pulsing at 70 Hz: one 2.86 ms long pulse for neutron spallation would be followed by four 0.7 ms long H^- pulses, with a distance of 1/70 ms between each pulse. The Radio-Frequency (RF) cavities in the ESS linac runs at 352.21 MHz in the low-energy section (up to 206 MeV) and 704.42 MHz in the medium- and high-energy section (from 206 MeV to 2 GeV).

Existing H^- sources have less intensity and less energy at extraction than requirements [7]. Therefore, a high intensity ion source for the ESSnuSB has to be developed.

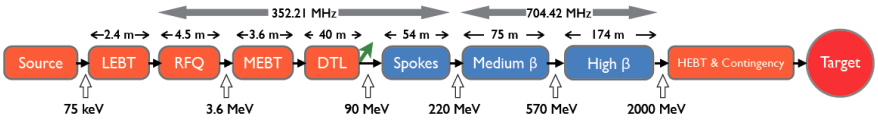

Figure 1.2: The ESS linac. The H^- beam is injected from the source and accelerated up to 2 GeV. A beam transport line leading to the accumulator ring will be installed at the end of the linac [8].

The Low-Energy Beam Transport (LEBT) leads the beam from the ion source to the Radio-Frequency Quadrupole (RFQ). The beam is directed towards the RFQ by using a chopper, two electrical plates, that is activated only after the ion source has stabilised in order to avoid that particles outside the energy acceptance reaches the RFQ. Due to the lower energy, an electron gas is used to mitigate defocusing space charge forces. In the RFQ, the beam is focused transversely, bunched, and accelerated [9]. The Medium Energy Beam Transport (MEBT) steers the beam from the RFQ to the Drift-Tube Linac (DTL), provides focusing and transverse collimation (reducing the transverse size of the beam by removing halo particles). It also contains instruments for beam diagnostics, which is essential to guarantee the quality of the beam. The Drift-Tube Linac (DTL) consists of a number of drift-tubes. A time-varying Radio Frequency (RF) electric field accelerates the beam between the drift-tubes and changes direction while the beam is inside the drift-tubes to avoid deceleration by the field in opposite direction. In the superconducting spokes cavities the beam

is accelerated from 79 MeV to 220 MeV by an accelerating gradient of 8 MV/m. Finally, the beam is accelerated up to the design energy of 2 GeV in elliptical superconducting cavities. After the end of the linac space is provided for future upgrades to higher energies.

At the end of the linac, the protons will continue towards a neutron spallation target, while the H^- will be deflected and led via an accumulator ring to the pion-producing target station. The target consists of small titanium spheres cooled with a high flow of cold helium gas. When the protons in the beam interact with the nuclei in the target, charged pions are produced. Negative (positive) pions decay into negative (positive) muons and muon antineutrinos (neutrinos), which in turn decay into electrons (positrons), muon neutrinos (antineutrinos), and electron antineutrinos (neutrinos) [4].

$$\pi^+ \rightarrow \mu^+ + \nu_\mu \tag{4}$$
$$\mu^+ \rightarrow e^+ + \nu_e + \bar{\nu}_\mu \tag{5}$$
$$\pi^- \rightarrow \mu^- + \bar{\nu}_\mu \tag{6}$$
$$\mu^- \rightarrow e^- + \bar{\nu}_e + \nu_\mu \tag{7}$$

The charged pions have a lifetime of about 2.6×10^{-8}, while muons have a lifetime of 2×10^{-6} [10]. A decay tunnel located downstream of the target will be long enough (25 m) for the pions to decay but at the same time short enough to not allow the longer lived muons to decay. To direct the resulting muon neutrino beam toward the detector, the pions are focused by a pulsed magnetic hadron collector, or horn. The horn needs to be pulsed with a current of 350 kA, which can only be provided in pulses of a few μs, which requires that the 0.7 ms beam is shortened to the same length using an accumulator ring.

1.3 THE ACCUMULATOR RING

From the end of the linac, the H^- pulse is led trough a beam transport system and injected into the 376 m circumference accumulator ring in order to compress the beam pulse to the required length. A stripping system located at the injection point will remove the electrons from the H^- to create a proton beam. The revolution time around the accumulator is much smaller than the pulse length, 1.32 μs compared to 0.7 ms. The beam is therefore accumulated during 530 turns.

Once the accumulator is filled, the beam circulating in the ring is extracted in one turn using a fast deflector magnet, a kicker. The magnetic field of a kicker has a rise time of at least 100 ns. To avoid that the beam is deflected into the vacuum chamber wall while the magnetic field is rising to full strength, it is necessary that there be a gap in the beam. This gap needs to be created in the linac using a

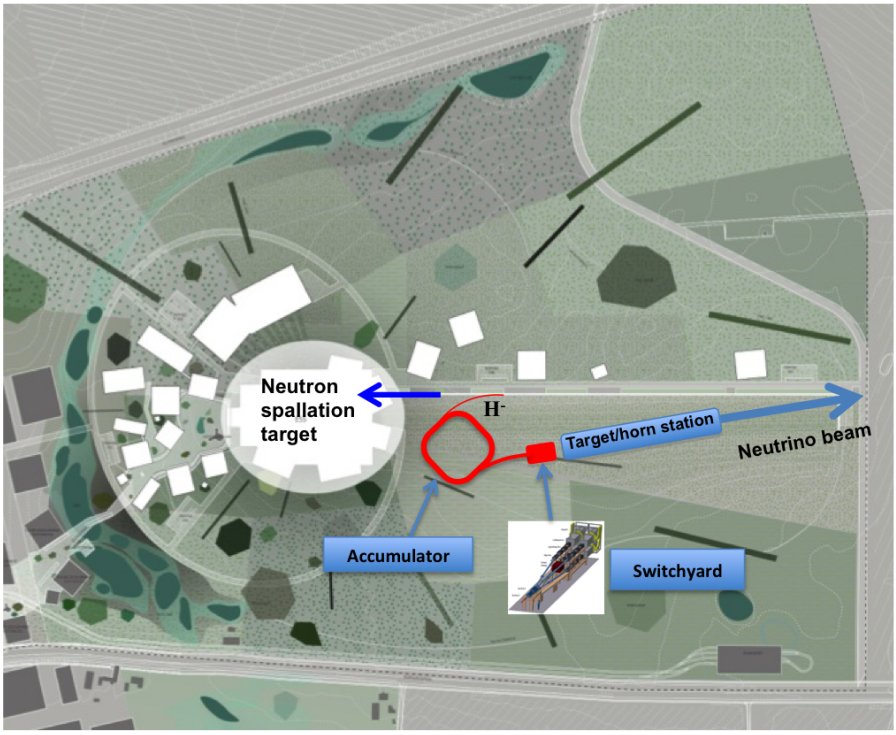

Figure 1.3: Sketch of a possible extension of the ESS site with the accumulator ring and target. The neutrino beam will be directed towards the detector site [11].

chopper, creating gaps in the beam at regular intervals corresponding to the circumference of the accumulator.

There are a number of technical challenges when designing the accumulator ring, related to the high intensity of the beam. In every step, beam losses and radiation need to be minimized. In this report, three of the most important challenges will be discussed.

- The high number of protons in the accumulator ring causes defocusing space charge effects, due to the Coulomb repulsion between the positively charged protons. This may cause instabilities and beam losses.
- The lifetime of the thin carbon foils used to strip the H^- to protons decreases with temperature. This sets limits to the tolerable beam density on the foil. Existing and future technologies need to be evaluated to solve this problem.
- A lattice for the accumulator ring that can provide a beam on target with the required parameters needs to be designed.

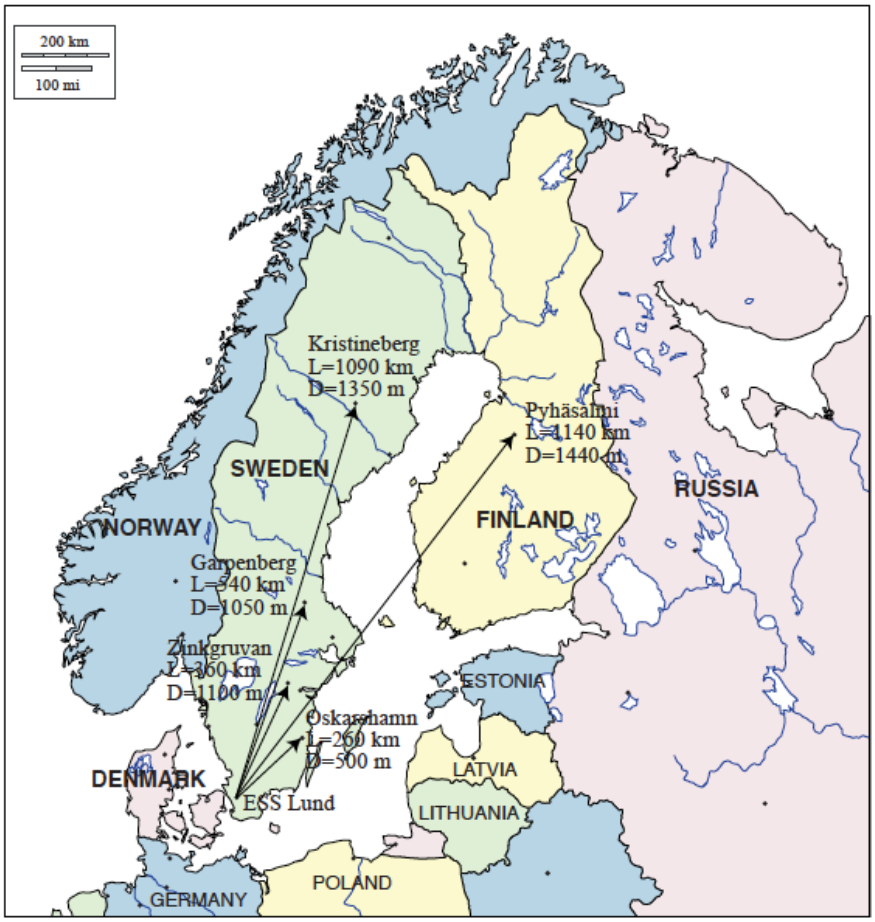

Figure 1.4: Map showing possible locations of the far detector. The current baseline is using the Garpenberg mining site located 540 km from Lund [8].

2

BEAM DYNAMICS AND SPACE CHARGE

In the accumulator ring, the beam circulates 530 turns before being ejected. This requires that the beam is stable throughout the accumulation period, in order to minimize losses and particle radiation. In this chapter, elementary beam dynamics and the concepts of tune and resonance instabilities are introduced. The tuneshift caused by the internal repelling space-charge force is discussed, and the results are applied to the ESSnuSB accumulator. Finally, the implications on the design of the accumulator are discussed in the end of the chapter.

2.1 BEAM DYNAMICS IN AN ACCELERATOR

The coordinate system in a circular particle accelerator is fixed as in figure 2.1. The reference frame moves around the closed orbit (defined as the orbit where a particle with ideal momentum comes back to it's exact initial condition after one turn).

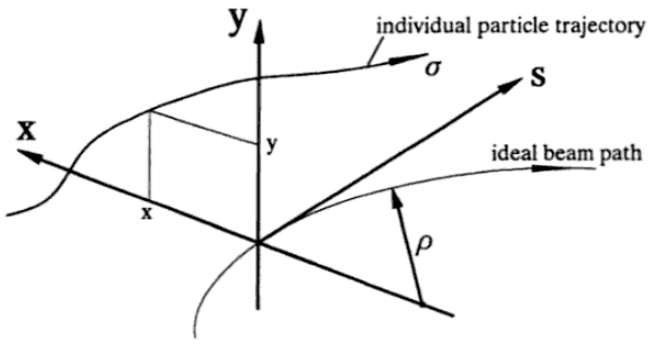

Figure 2.1: Coordinate system in an accelerator: x is the horizontal component, y is the vertical component, s is the component along the beam direction, and ρ is the radius of the ideal beam path, the design orbit. Individual particles may undertake orbits around the ideal orbit [14].

In a particle beam, each particle undergoes an oscillation in the x, y-plane around the closed orbit when travelling along the accelerator. This transverse movement is described by Hill's equation [12]:

$$y'' + K(s)y = 0. \tag{1}$$

This resembles the spring equation, with a spring potential K that depends on the distance s. The restoring force is coming from the focusing magnets which are placed around the ring. Since the ring is circular, K must be a periodic function $K(s+L) = K(s)$. A solution of (1) is given by:

$$y = \sqrt{\beta(s)\epsilon}\cos[\phi(s) + \phi(0)], \tag{2}$$

where $\beta(s)$ is called the *beta function*, and it is related to the maximum transverse amplitude at each point around the ring. $\phi(s)$ is the phase, $\phi(0)$ the initial phase, and ϵ is an amplitude constant. Every particle has a different amplitude, but ϵ is the amplitude constant for which, generally, 68% of the particles have a smaller amplitude, and it is called the *emittance*. Since β depends only on the distance s along the trajectory of the particle, it is the same for every particle in the beam. The maximum possible amplitude is when $\cos[\phi(s) + \phi(0)] = 1$ and it is given by

$$y_{max} = \sqrt{\beta(s)\epsilon}. \tag{3}$$

This is the radial beam size as a function of s. For a beam with a given ϵ and β, this represents the minimum beam chamber aperture size which can host the beam inside. Inversely, a given aperture and β defines the maximum ϵ that can fit inside the beam chamber. The smallest value of ϵ in the machine, called the acceptance, defines the maximum beam emittance that can fit inside the accelerator.

With the current baseline, the ESSnuSB accumulator ring will have an emittance of 37.5 mm-mrad. The beam chamber must have an inner radius of at least 10 times the amplitude to minimize beam loss:

$$r_{aperture}[m] \approx 10\sqrt{\beta(s)\cdot 37.5\times 10^{-6}}. \tag{4}$$

2.1.1 *Tune and resonance*

The number of oscillations a particle makes around the closed orbit in each turn is called *tune*. In a real machine, there are always errors due to magnet misalignment and focusing field imperfections. If the tune is an integer, the particle will see the same error each turn, so the errors will build up quickly and the particle may be lost. If the fractional part of the tune is half-integer, the particle will see the same error every two-turns, for fractional part of $1/3$ every third turn and so on for other rational numbers. This means that there are several "forbidden values" or resonances (see further below) for the tune that

will not give a stable beam. The tune depends on the focusing of the magnets; stronger focusing gives a higher tune, and vice versa.

Inserting the solution (2) to Hill's equation into the original equation (1) yields

$$\sqrt{\epsilon}\left[\frac{\beta''(s)}{2\sqrt{\beta(s)}} - \frac{\beta'^2(s)}{4(\beta(s))^{3/2}} - K(s)\sqrt{\beta} - \phi'^2(s)\frac{\beta'(s)}{2\sqrt{\beta}}\right]\cos(\phi(s)+\phi(0))$$
$$-\sqrt{\epsilon}\left[\phi''(s)\sqrt{\beta} + \frac{\phi(s)\beta'(s)}{2\sqrt{\beta}}\right]\sin(\phi(s)+\phi(0)) = 0.$$

Requiring that this equation holds for all values of s, the expressions between the brackets must be zero. This yields the necessary conditions:

$$\frac{\beta''(s)}{2\sqrt{\beta(s)}} - \frac{\beta'^2(s)}{4(\beta(s))^{3/2}} - K(s)\sqrt{\beta(s)} - \phi'^2(s)\sqrt{\beta(s)} = 0 \tag{5}$$

$$\phi''(s)\sqrt{\beta(s)} + \frac{\phi(s)\beta'(s)}{\sqrt{\beta(s)}} = 0. \tag{6}$$

From equation (6) comes the following relation between the phase advance and the beta function, which can be found after integration [13]:

$$\phi(s) = \int_0^s \frac{ds}{\beta(s)}.$$

This requires that $\beta(s)$ is nonzero for all s along the ring, which is true (see for example [14]). The phase advance for one turn $\phi(2\pi R)$ is equal to $2\pi Q$, where Q is the tune. The tune is thus defined by

$$Q = \frac{1}{2\pi}\oint_0^{2\pi R} \frac{ds}{\beta(s)}. \tag{7}$$

Equation (7) simply states that for big values of β, the oscillation amplitude is bigger and therefore takes longer time, which decreases the number of oscillations in one turn. For small values of β, oscillations are smaller which increases the tune. To avoid beam instabilities, it is important that the vertical and horizontal tunes do not produce a resonance: $nQ_x + mQ_y = k$, where k is a rational number. The lines indicating forbidden tunes are often depicted in a *tune chart* (see figure 2.2).

2.1.2 *Dispersion*

So far, only particles with ideal momentum, $\Delta p = 0$, have been considered. In a real machine, however, the particles always have $\Delta p \neq 0$

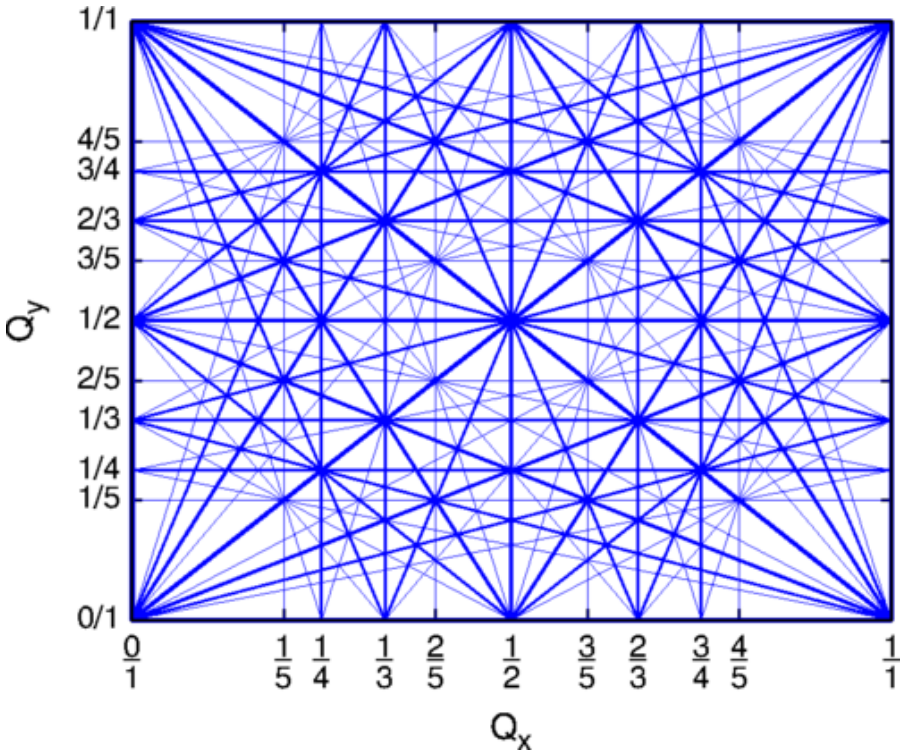

Figure 2.2: Tune chart. The blue lines, called stopbands, indicate resonance lines and the boldness indicate the strength of the resonance[15]. The fractional part of the tune should avoid places where any resonances may appear. This is in general impossible, since the beam covers a finite area in the tune chart.

and this induces dispersion. Off-momentum particles sees a driving term in the Hill equation [12]:

$$y'' + K(s)y = -\frac{1}{\rho(s)}\frac{\Delta p}{p}. \tag{8}$$

Where $\rho(s)$ is the curvature radius, Δp the momentum error, and p the design momentum. Therefore, dispersion is nonzero only when particles are being bent (for a straight trajectory, $\rho = \infty$). When the particles are bent, for example by a magnet in an accelerator, the effect is similar to that of a prism in optics; higher-momentum particles are bent less than the particle with ideal momentum, and lower-momentum particles are bent more. The dispersion function $D(s)$ is defined as the the particular solution to (8). A more general discussion can be found in references [16], [12], and [14], but the most important result is that the beam size increases whenever there is dispersion:

$$y_{max} = \sqrt{\beta_y(s)\epsilon_y + D_y^2(s)\left(\frac{\Delta p}{p}\right)^2}. \tag{9}$$

This is one of the reasons why dispersion should be minimized, or zero, whenever a small beam size is necessary. One way of suppressing dispersion in the straight sections that will be used in the design of the ring, is to enforce a phase advance of an integer times 2π in all bending arcs [16]. This is because the dispersion is a periodic function, and will return to zero after a full period.

The inner radius of the beam chamber of the ESSnuSB accumulator ring, found in equation (4) can now be accounted to account for dispersion:

$$r_{\text{aperture}}[m] \approx 10\sqrt{\beta(s)\cdot 37.5\times 10^{-6} + D^2(s)\left(\frac{\Delta p}{p}\right)^2}, \tag{10}$$

where $\beta(s)$ is the beta function at position s in the machine, D the dispersion function, and $\Delta p/p$ the momentum deviation, which will depend on the final design of the accumulator.

2.2 SPACE CHARGE TUNE SHIFT

In a charged particle beam, the individual particles are repelled from each other, which defocuses the beam. At the same time, the charged particles move in the longitudinal direction which creates a magnetic self-field that creates an inward, focusing force. At the speed of light, these two effect are equal and completely cancel. Below the speed of light, the repelling force dominates which causes a focusing error. This focusing error leads to a tune shift, which can cause some particles to pass into resonance tunes and be lost in the accelerator. The tune shift caused by a focusing error ΔK can be calculated by [17]:

$$\Delta Q_y = -\frac{1}{4\pi}\int_0^{2\pi R} \Delta K_y(s)\beta_y(s)\,ds, \tag{11}$$

where ΔQ_y is the tune shift in the y-direction, and $\beta_y(s)$ is the beta function. This equation is true for both the x and y transverse directions. ΔQ should be kept below 0.2 to minimize the number of particles that pass into resonance [17].

To find an expression for $\Delta K(s)$, Hill's equation with no outside focusing and defocusing effects due to space charge can be considered:

$$y'' - \Delta K(s)y = 0. \tag{12}$$

y'' is the second derivative of y with respect to s. It can also be expressed in terms of the temporal derivative:

$$y'' = \frac{d^2y}{ds^2} = \frac{d^2t}{ds^2}\frac{d^2y}{dt^2} = \frac{1}{\beta^2c^2}\frac{d^2y}{dt^2}. \tag{13}$$

Replacing y'' with $\Delta K(s)y$ (from (12)) yields [17]:

$$\frac{1}{\beta^2 c^2}\frac{d^2 y}{dt^2} = \frac{1}{\beta^2 c^2}\frac{F_y}{m_0\gamma} = \Delta K(s) y \tag{14}$$

$$\Rightarrow \Delta K(s) = \frac{1}{\beta^2 c^2}\frac{F_y}{m_0\gamma}\frac{1}{y}. \tag{15}$$

Thus, $\Delta K(s)$ can be expressed in terms of the space charge force acting on a particle. This force is the sum of the defocusing electric force and the focusing magnetic force. In the following, an unbunched circular beam with a gaussian particle distribution in the transverse plane will be assumed. A bunched beam would increase the tune shift as calculated here. The gaussian distribution is used because it is more realistic than the uniform particle distribution [17].

The particle distribution in a gaussian beam is given by

$$\eta(r) = \frac{I}{2\pi\beta c\sigma^2} e^{-r^2/2\sigma^2} \tag{16}$$

$$r = \sqrt{x^2 + y^2}, \tag{17}$$

where I is the beam current, c the speed of light, σ the spread, and r the radius from the center of the beam to a test particle inside the beam. This yields the following electric and magnetic fields [17]:

$$\mathbf{E} = E_r \hat{e}_r = \frac{I}{2\pi\epsilon_0\beta c r}\left[1 - e^{-r^2/2\sigma^2}\right] \tag{18}$$

$$\mathbf{B} = B_\theta \hat{e}_\theta = \frac{I}{2\pi r c^2 \epsilon_0}\left[1 - e^{-r^2/2\sigma^2}\right], \tag{19}$$

where ϵ_0 the vacuum permittivity. The Lorentz force acting on a positively charged test particle is

$$F_L = e[\mathbf{E} + \boldsymbol{v} \times \mathbf{B}]. \tag{20}$$

Since the particle velocity is much smaller in the transverse directions than in the longitudinal direction, the following approximation can be made:

$$v_{x,y} \ll v_s \Rightarrow \boldsymbol{v} \approx v_s \hat{e}_s = \beta c \hat{e}_s$$

.

So that, in a cylindrical coordinate system:

$$\boldsymbol{v} \times \mathbf{B} \approx -v_s B_\theta \hat{e}_r = -\beta c B_\theta \hat{e}_r. \tag{21}$$

By substitution of the expressions for the electric field (in eq. (18)), the magnetic field (in eq. (19)), and the approximation of the cross product $\boldsymbol{v} \times \mathbf{B}$ (in (21)), the expression for the Lorentz force (20), becomes [17]:

$$F_r(r) = e\left[\frac{I}{2\pi\beta c r}\left[1 - e^{-r^2/2\sigma^2}\right] - \beta c \frac{I}{2\pi r c^2 \epsilon_0}\left[1 - e^{-r^2/2\sigma^2}\right]\right] \quad (22)$$

$$= \frac{Ie}{2\pi r \epsilon_0 \beta c \gamma^2}\left[1 - e^{-r^2/2\sigma^2}\right]. \quad (23)$$

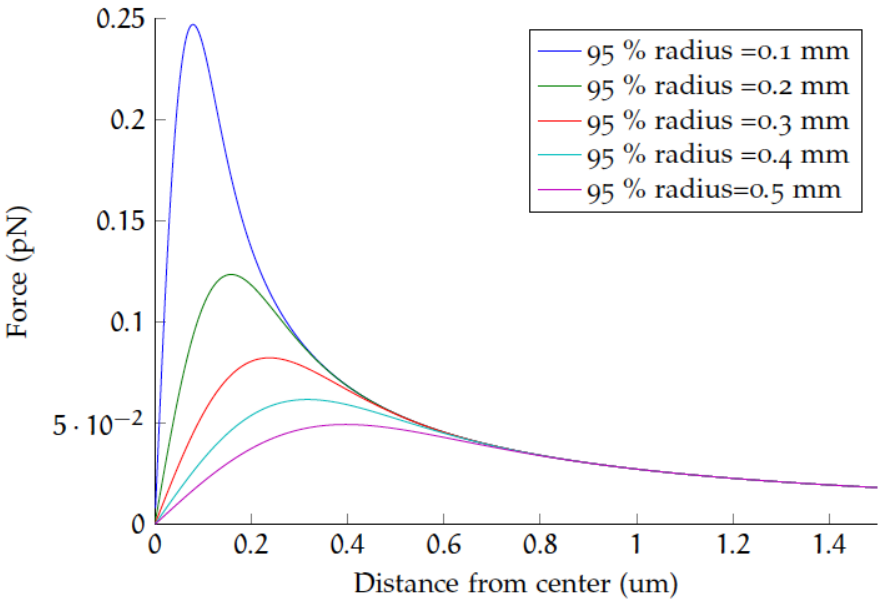

Figure 2.3: Defocusing Lorentz force as a function of radius for a 1D gaussian-distributed beam with different beam sizes. Note that the beam size is not constant in an accelerator due to focusing, so the defocusing force depends on the position in the machine.

This result is plotted in figure 2.3. As is clearly seen the space charge force is strongest for particles near the beam center while it is zero for particles in the beam center. It is therefore useful to linearize equation (23) for small r. This yields, using the expansion of $e^{-x^2} = 1 - x^2 + O(x^4)$ [17]:

$$F(r) = \frac{Ie}{2\pi r \epsilon_0 \beta c \gamma^2}\left[1 - 1 + r^2/2\sigma^2 + O(x^4)\right] \approx \frac{Ie \cdot r}{2\pi\epsilon_0 \beta \gamma^2 2\sigma^2}. \quad (24)$$

ΔK can now be found by using the linearized expression for the space charge force (24) in equation (15) (assuming that the force is in the horizontal y-direction):

$$\Delta K(s) = \frac{1}{\beta^2 c^2}\frac{F_y}{m_0 \gamma}\frac{1}{y} = \frac{1}{\beta^2 c^2 m_0 \gamma}\frac{Ie \cdot y}{2\pi\epsilon_0 \beta c \gamma^2 c 2\sigma^2}\frac{1}{y} = \frac{N r_0}{R\pi\beta^2\gamma^3 2\sigma^2}, \quad (25)$$

where $r_0 = e^2/(4\pi\epsilon_0 m_0 c^2) = 1.54 \times 10^{-18}$ is the classical proton radius and I has been replaced by $Ne\beta c/2\pi R$. The tune shift ΔQ_y is then, according to equation (11):

$$\Delta Q_y = -\frac{1}{4\pi}\int_0^{2\pi R} \frac{N r_0}{\pi R \beta^2 \gamma^3 2\sigma^2}\beta_y(s)\,ds. \tag{26}$$

This integral can be approximated by using the so-called smooth approximation, using that the mean value $\langle \beta(s)/\sigma^2 \rangle$ is equal to the inverse of the Root Mean Square (RMS) beam emittance [17], from the expression of beam size found in (3): $\sigma = \sqrt{\beta \epsilon_y}$. Formally,

$$\frac{1}{2\pi R}\oint_0^{2\pi R} \frac{\beta_y(s)\,ds}{\sigma^2} = \left\langle \frac{\beta_y(s)}{\sigma^2} \right\rangle = \frac{1}{\epsilon_y}.$$

Rewriting equation (26):

$$\begin{aligned}
\Delta Q_y &= -\frac{1}{2\pi R}\int_0^{2\pi R} \frac{N r_0}{\pi \beta^2 \gamma^3}\frac{\beta_y(s)}{4\sigma^2}\,ds \\
&= -\frac{N r_0}{4\pi R \beta^2 \gamma^3}\left\langle \frac{\beta_y(s)}{\sigma^2} \right\rangle \\
\Rightarrow \Delta Q_y &= -\frac{N r_0}{4\pi \beta^2 \gamma^3}\frac{1}{\epsilon_y}.
\end{aligned}$$

Here, ϵ_y is the so-called geometrical emittance. The geometrical emittance shrinks with increasing energy, it is therefore usual to define the normalised emittance, $\epsilon_{n,y} \equiv \epsilon_y \beta\gamma$, which is independent of energy [14]. With this definition, the space charge tune shift finally becomes

$$\Delta Q = -\frac{N r_0}{4\pi \beta\gamma^2}\frac{1}{\epsilon_{n,y}}. \tag{27}$$

A calculation based on the ideal case of a uniform particle distribution would have given a result half as big [17].

In the ESSnuSB accumulator ring, a very high number of protons will be stored, and so even a fractionally small beam loss leads to heavy radiation of the accelerator equipments. For this reason, keeping the tune shift below 0.2 is important to avoid beam losses [8].

2.2.1 *Method*

The space charge parameters needed to calculate the tune shift in the ESSnuSB are listed in table 1.

The γ and β coefficients were calculated by using

$$\gamma = \frac{E_k}{m_0 c^2} + 1$$

$$\beta = \sqrt{1 - \frac{1}{\gamma^2}},$$

	NAME	VALUE	UNIT
N	Number of protons	2.8×10^{14}	protons
$\epsilon_{n,y}$	Normalised RMS beam emittance	37.5	mm-mrad
β	Beam velocity	0.95	c
γ	Relativistic factor	3.13	1

Table 1: Parameters for the ESSνSB, taken from [8]

where the kinetic energy E_k is 2 GeV and the rest mass m_0 is 938 MeV/c^2 for protons ($c = 1$ in these units).

In [8], a value of 0.75 was found for the space charge tune shift for one accumulator ring, at 2.5 GeV kinetic energy (the previous ESS design energy [6]), 14 Hz and a RMS emittance of 25 mm-mrad. Two solutions have been proposed to mititage the space charge effects. Building four rings, while keeping the ESS linac pulsing, i.e. 14 Hz for protons and 14 Hz for $H^-$to decrease the intensity, and therefore the maximum tune spread, by a factor of 4, keeping the same emittance [8]. Another solution being studied proposes to increase the linac pulsing to 70 Hz, with one proton pulse followed by four H^-pulses. This would also decrease the maximum tune shift by a factor of 4 [18].

2.3 RESULTS AND CONCLUSIONS

The values from table 1 used in equation (27) give a tune shift of 0.0968, with a 2D circular gaussian-distributed beam. While not final, these results give an estimation of the tune shift in the accumulator. This is well below the threshold tune shift of 0.2. The tune shift would be increased by considering a bunched beam, so a more detailed study should include this effect. It should also be noted that the tune shift of 0.75 as calculated in the section above refers to the old baseline where one H^-pulse was accelerated between each proton pulse, instead of four.

Another important conclusion from this chapter is that dispersion can be suppressed by forcing a phase advance of an integer times 2π in the bending arcs of the accumulator. This will be used in the lattice design in chapter 4.

3

INJECTION INTO THE ACCUMULATOR RING

The goal of this chapter is to study the injection and stripping process into the ESSnuSB accumulator ring. Two different injection schemes are discussed. Multiturn injection is used to inject a proton beam on a proton beam, which induces significant particle losses. Charge exchange injection instead injects H^-on protons and is less lossy than multiturn injection. However, it requires an effective method to strip the electrons from the H^-after injection. Thin carbon foils are already in use in similar machines for this purpose, but the foils are heated and damaged by the traversing particle beam. The maximum temperature induced by the beam on the carbon foil is simulated using a computer model in section 3.2.

3.1 MULTITURN AND CHARGE EXCHANGE INJECTION

In the accumulutor ring, the beam is injected during a few hundred turns, depending on the circumference on the ring. As mentrioned above, two common injection schemes are *multiturn injection* and *charge exchange injection*. In both injection schemes a set of bumper magnets is used to create a local bump in the closed orbit of the accumulator. In multiturn injection, protons are injected on protons, and the injected beam is brought parallel to the circulating beam using as septum magnet (see figure 3.3). This causes beam losses since the outer particles in the circulating beam will hit the outside of the septum magnet and be lost. In charge exchange injection, $H^-$are injected on protons and the electrons are removed using a thin stripping foil (see figure 3.4). The advantage of the charge exchange method is that the two beams can be bent in the same magnet, due to their different charge. This avoids placing a septum magnet close to the circulating beam and is therefore considerably less lossy [13].

The area the beam occupies in transverse phase space, called emittance, is conserved due to Liouvilles theorem. In multiturn injection, the injected beam is painted in transverse phase space from the center out. In charge exchange injection, it is not necessary to paint since H^-does not occupy the same phase space as protons because of their different charge. However, an increased emittance, up to 37.5π mm-

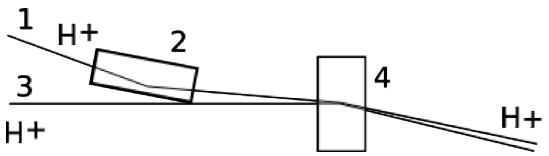

Figure 3.1: Multiturn injection. The incoming proton beam (1) is bent in the septum magnet (2) almost parallel to the circulating beam (3). They are bent together down to the closed orbit in a dipole (4). The two beams are not bent perfectly parallel since they enter the dipole with different angles [19].

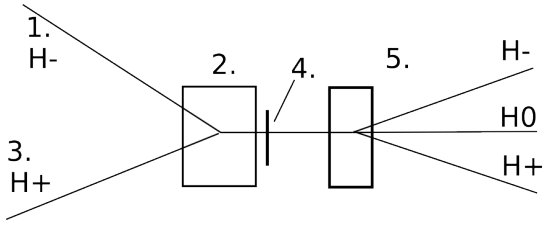

Figure 3.2: Charge exchange injection. The incoming H^- beam (1) is bent in a dipole (2) together with the circulating beam (3). Due to their different charge, the two beams can be bent in the same magnet. A stripping foil (4) removes the extra electrons from the H^-. Another dipole (5) bends the combined beam to the closed orbit. The unstripped H^0 and H^- are led to a beam dump [19].

mrad is advantageous in ESSnuSB due to space charge forces (see chapter 2).

3.2 FOIL STRIPPING

One of the most important challenges for the ESSnuSB accumulator ring is the injection stripping process, where the two extra electrons are removed from the H^- beam. A frequent technique is to use thin carbon stripper foils, but foils suffer from limited lifetime due to heating and mechanical damage from the beam. Replacing the foil is a costly and time-demanding process. Laser stripping has been proposed as an alternative to foil stripping [19]. A high-intensity laser is focused on the beam and excites the electron to an outer orbit, where it can be removed using magnets with high enough fields. However, laser stripping is not yet a proven technology and there are still years of R&D [20] required before it can be implemented in a high-intensity machine, compared to foil stripping which is a proven technique that can be relatively straightforwardly implementated.

In modern-day machines, carbon is the material of choice for stripping foils. The advantages of carbon are that it has a high melting point, that it is mechanically durable, and that it brings comparatively little perturbations to the beam due to its low atomic weight

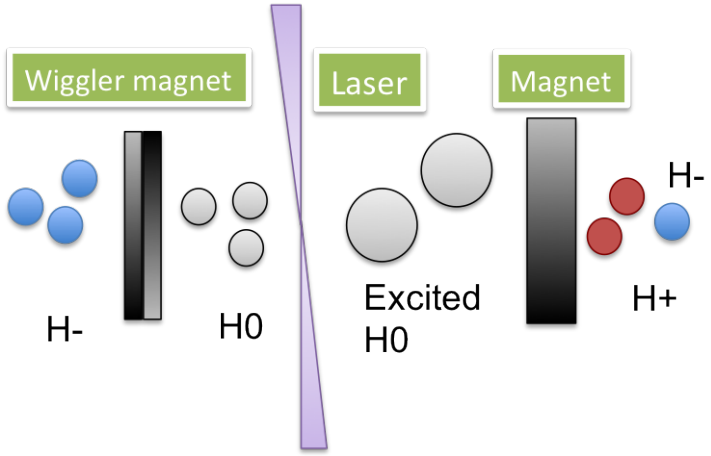

Figure 3.3: Laser stripping. A wiggler magnet removes the outer electron from the H^-. A laser then excites the second electron to an outer orbit, where it can be removed using another magnet [19].

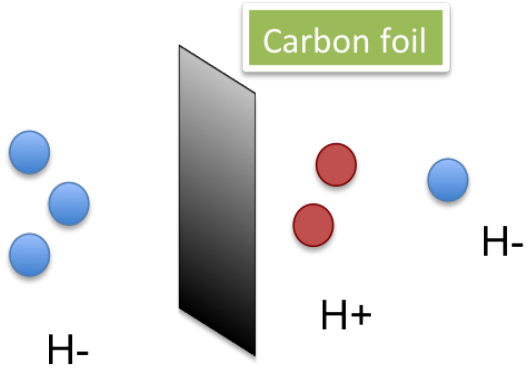

Figure 3.4: Foil stripping. A thin carbon foil strips away the electrons from the proton nucleus [19].

[21]. Recent developments in production techniques have allowed the production of foils with ever better durability and heat resistance [22].

For foil stripping, a thin carbon foil is mounted inside the beam tube. When H^- pass through the foil, the electrons are removed:

$$H^- \rightarrow H^+ + 2e^-$$
$$H^- \rightarrow H^0 + e^-$$

Some of the H^- also remain as H^-. After the foil, another magnet sorts out the H^- and H^0 particles, while the H^+ remains in the closed orbit [23]. The beam deposits a fractional part of it's energy when it passes through the foil. This interaction with the beam heats the foil which causes the carbon to evaporate, reducing the thickness and decreasing the lifetime. The major factors that determine the foil lifetime are beam current density, foil thickness, and foil preparation method. There are different processes that dominate the foil destruc-

tion: for temperatures below 800 K, radiation damage dominates. For temperatures over 1300 K, the deplacement of the crystal atoms by the incident beam dominate the process [24]. For temperatures under 2500 K, increasing the thickness increases the lifetime [21]. Foil lifetime is significantly reduced for temperatures over 2500 K, and so this sets a practical goal for the design [25].

The temperature on the foil is governed by the heat equation [24]:

$$\nabla^2 T_c + \frac{1}{k_c t_c}[P - 2\sigma f \epsilon_c (T_c^4 - T_0^4)] = \frac{1}{\alpha_c}\frac{\delta T_b}{\delta \tau}. \tag{1}$$

where $\alpha_c = k_c/\rho_c c_c$, and k_c, ρ_c, and c_c are the thermal conductivity (W/m-K), the foil density (kg/m^3), and the carbon heat capacity (J/Kg-K), respectively. P is the beam power density (W/m^2), t_c the foil thickness (g/cm^2), T_c is the foil temperature (K), T_0 the ambient temperature (K), σ the Boltzmann constant, f the radiation view factor, and τ is the time (s). A reduced form of (1) can be found by assuming no heat diffusion across the foil ($\nabla^2 T \to 0$), constant foil thickness, and no heat radiation from the beam pipe to the foil. Only heat radiation from the foil is considered as a cooling effect, and the heating is determined by the power density of the incident beam:

$$\frac{dT_c}{d\tau} = \frac{-2\sigma f \epsilon_c (T_c^4 - T_0^4) + P}{\rho_c t c_c}. \tag{2}$$

To calculate the power density the following formula can be used [24]:

$$P = \frac{I \cdot S_P}{\sigma_D}, \tag{3}$$

where I is the beam current (A), σ_D the beam cross section (m^2), and S_P is the stopping power (MeV/cm). NIST, the National Institute of Standards and Technology, provides two online databases with values for the stopping power: Pstar [26] for protons and Estar [27] for electrons (see table 1) . The database uses a mix of theoretical formulas and interpolations from experiments to calculate the values of the stopping power in different materials. Amorphous carbon with a density of 2000 kg/m^3 is used as foil material in the simulations. The stopping power for protons is plotted as a function of energy in figure 3.5, and for electrons in figure 3.6. The proton has approximately the same energy as the H^-, 2 GeV, because it is 2000 times heavier than the electrons, orbiting the proton in the H^-.

To account for the two electrons in the, H^-, their kinetic energy is calculated. The electrons move with the same speed as the protons, so they have the same β (the fraction of the speed of light) and γ, which is the Lorentz factor calculated as

$$\gamma = E_p/m_p + 1, \tag{4}$$

where E_p is the kinetic energy for protons and m_p is the proton mass. The electron kinetic energy is:

$$E_e = m_e(\gamma - 1). \tag{5}$$

	PROTONS	ELECTRONS	H^-
Kinetic energy (GeV)	≈ 2	1.0896	2
Mass (MeV/c^2)	938	0.511	≈ 938
Stopping power (MeV cm^2/g)	1.763 [26]	1.611 [27]	4.9850

Table 1: Parameters used to calculate the stopping power of electrons, protons and H^- in amorphous carbon with a density of 2000 kg/m^3.

The total power deposited in the foil is found by multiplying the stopping power with the foil thickness t.

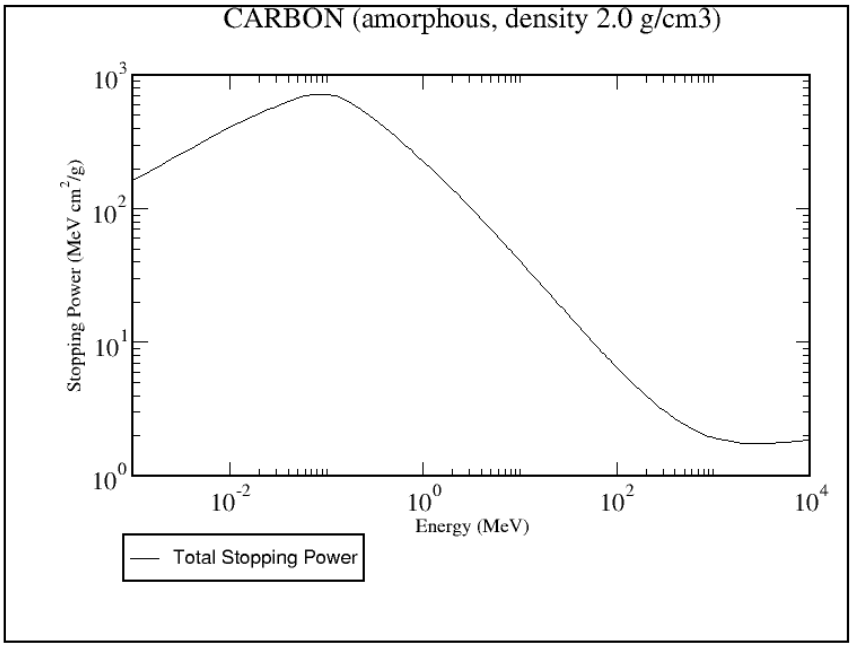

Figure 3.5: Stopping power of protons in carbon as a function of energy [26].

Finally, with unit brackets for clarity [24],

$$P\left[\frac{W}{m^2}\right] = 4.985\left[MeV\frac{cm^2}{g}\right]\cdot t\left[\frac{g}{cm^2}\right]\cdot I\,[A]\cdot\frac{1}{\sigma_D}\left[\frac{1}{m^2}\right].$$

The heat capacity c_c (J/kgK) is given by the polynomial approximation [28]:

$$c_c = 12.7 + 2.872T - 0.00145T^2 + 3.12\cdot 10^{-7}T^3 - 2.83\cdot 10^{-11}T^4. \tag{6}$$

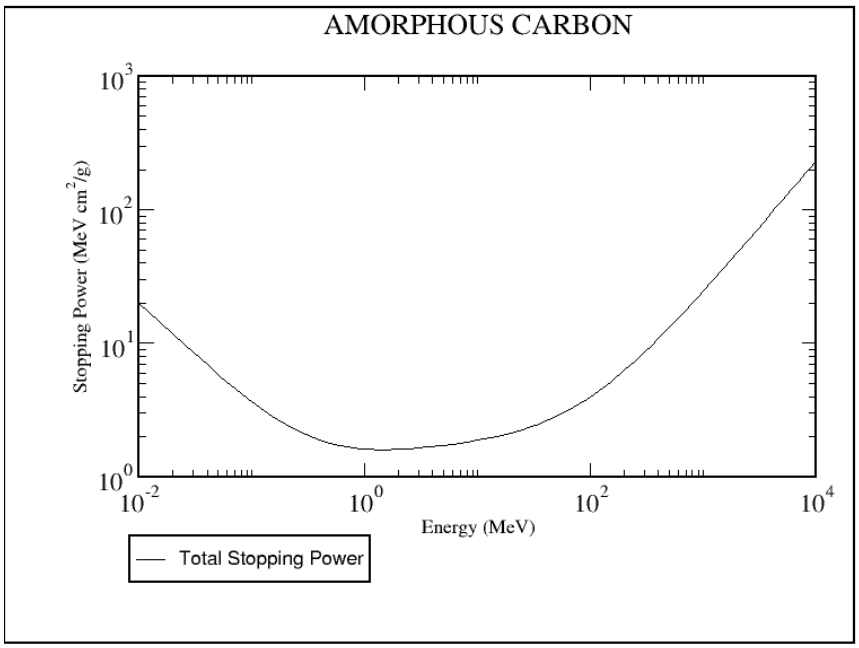

Figure 3.6: Stopping power of electrons in carbon as a function of energy [26].

3.2.1 *Method*

To solve (2), Matlab's ode15s was used. This numerical differential equation solver is well suited for the problem since the derivative changes quickly, causing the step size to be too small for other solvers.

Every new period, a new pulse is injected and the solution is restarted. As a new initial condition, the end temperature of the old solution is used. The simulation only includes heating effects from the injected beam and not the circulating beam; this is motivated by the fact the circulating beam has a much larger cross section than the injected beam and that it only partially overlaps the foil. This has been confirmed in particle tracking simulations by [31].

The problem was solved for different cases:

- One ring, 70Hz, protons only
- One ring, 70Hz, H^-
- Four rings, 14Hz, protons only
- Four rings, 14Hz, H^-

The difference between these scenarios is the frequency of the pulses, and considering the power deposition of H^-, including two electrons, or the proton power deposition, without electrons. The latter is interesting in the case of two or more stripping foils, since protons contributes less to heating than H^-. The problem is then solved for

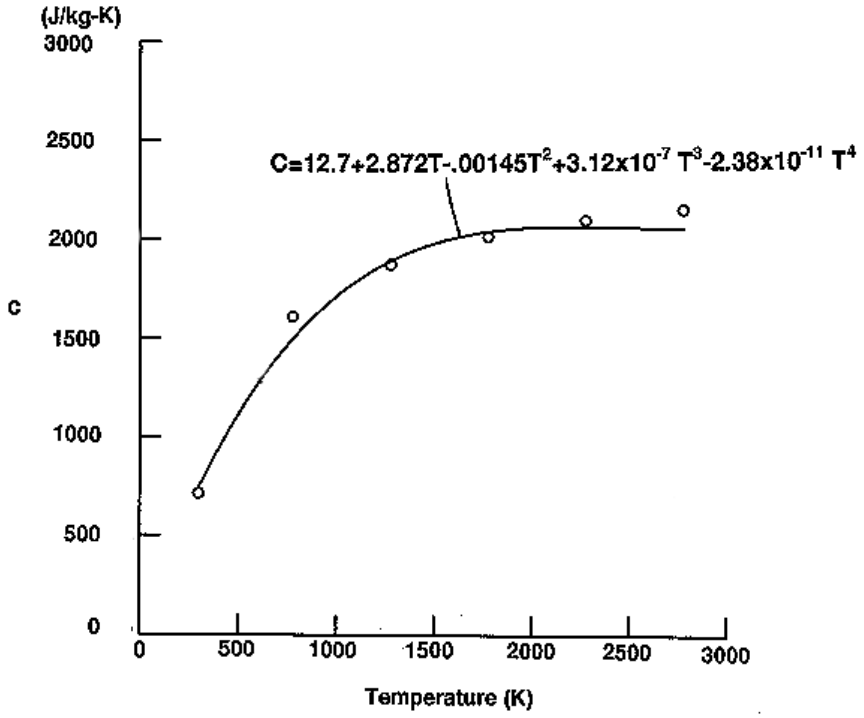

Figure 3.7: Experminentally measured carbon heat capacity as a function of temperature (circles) and polynomial approximation (line) [28].

different values of the beam spot size on the foil, to determine the necessary transverse size.

3.3 RESULTS AND CONCLUSIONS

The maximum foil temperatures for different beam spot sizes are plotted in figure 3.8. Note that the 70 Hz simulation slightly overestimates the temperature because every fifth pulse should be empty, corresponding to the proton pulse used for neutron spallation. A particular case, using a spot size of 8×10 mm^2 is plotted in figure 3.9. These preliminary results show that foil stripping could used in the ESSnuSB provided that the beam cross section on the foil can be made big enough. This is important since it can be implemented relatively straightforwardly, while an operational laser stripping system might not be available at the startup of ESSnuSB. A possible scenario is to start operating the accumulatur with a foil stripping and change to a laser stripping system once it is available.

While positive results were obtained using a simplified model, a more detailed study is required. The simplified model did not include the circulating beam, which is considerally more intense, but with a larger cross-section, than the injected beam. A more realistic sim-

	NAME	VALUE/UNIT	
T_c	Temperature on the carbon foil	K	
T_0	Ambient temperature	297 K	[28]
τ	Time	s	
A_c	Foil surface area	$17 \times 62\text{mm}^2$	[28]
σ_D	Beam size	$3.1 \times 1.6\ \text{mm}^2$	
ρ	Density (amorphous carbon)	$2000\ \text{kg/m}^3$	[26]
ϵ	Rad. Emissitivity (carbon)	0.8	[28]
f	Rad. view factor (carbon)	1	[28]
σ	Stefan-Boltzmann constant	$5.67 \times 10^{-8}\ \text{W/m}^2\text{K}^4$	[28]
P	Power density	W/m^2	
t_m	Foil thickness	$750\ \mu\text{g/cm}^2$	
I	Beam current	62.5 mA	[8]
	Revolution frequency	14 Hz	[8]
	Pulse length	0.7150 ms	[8]
S_P	Stopping power	$5.289\ \text{MeV}/(\text{cm}^2/\text{g})$	[26]
	Carbon melting point	3973 K	[29]

Table 2: Beam- and foil parameters used in the simulations

ulation should include the circulating beam aswell as the injection painting method, the geometry of the foil, and heat conduction across the foil. Preliminary results using more realistic models are so far in line with the results of the simplified model [30], [31]. Laser stripping should be continued to be studied as a replacement to foil stripping.

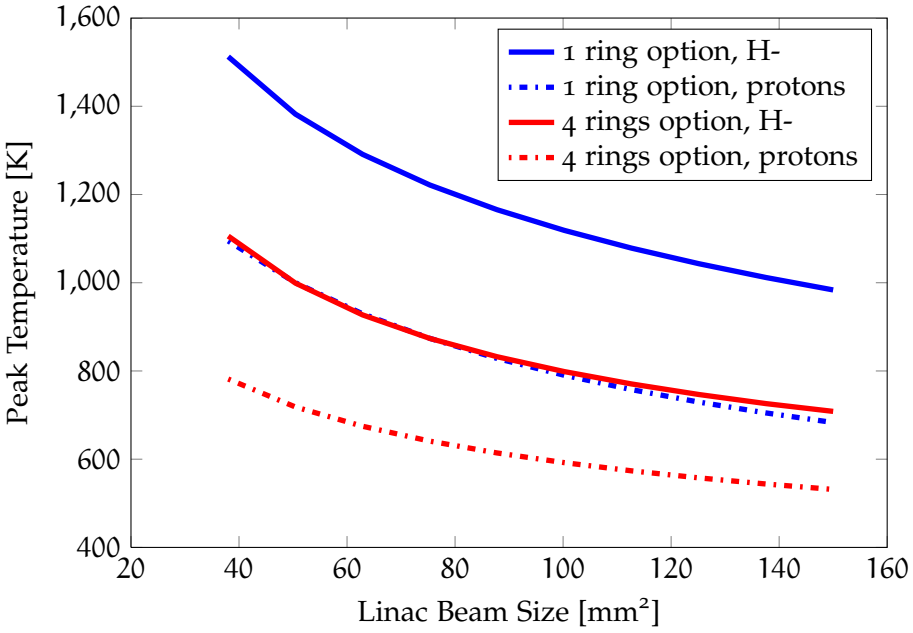

Figure 3.8: Maximum foil temperature as a function of time with one and four rings, as a function of linac beam spot size on the foil.

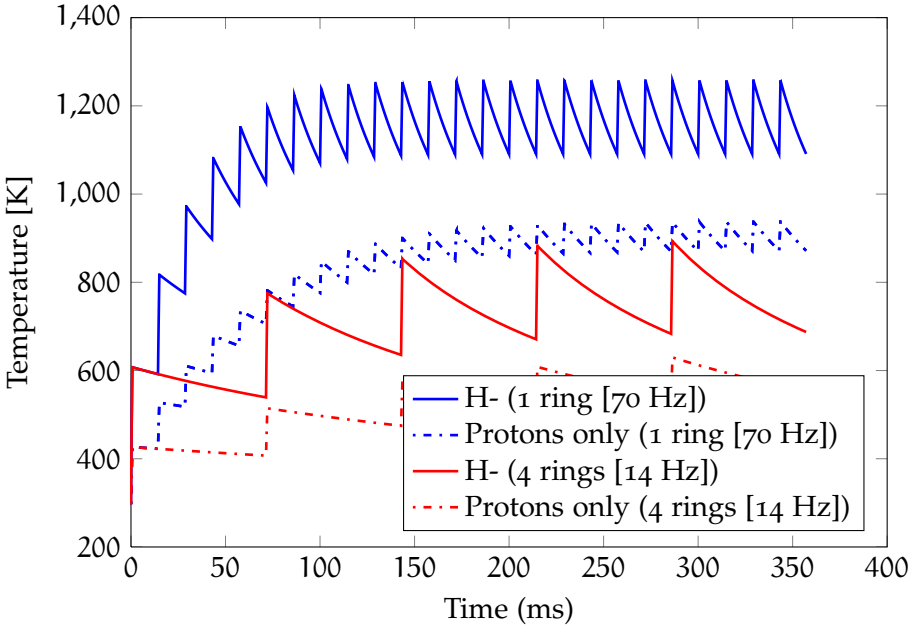

Figure 3.9: Foil temperature as a function of time with one and four rings, with a linac beam spot size of 80 mm^2.

4

LATTICE DESIGN

A particle accelerator fundamentally consists of a vacuum chamber in which the beam circulates, and magnets to bend and focus the beam. Electric fields, generated in pulsed Radio-Frequency (RF) cavities are used to accelerate the beam. The location, length, and strength of each element along the accelerator is called the lattice. The development of a first lattice for the ESSnuSB accumulator ring will be described here.

4.1 DESIGN GOALS AND CRITERIA

As mentioned in chapter 1, the purpose of the accumulator is to shorten the beam pulse from 0.7 ms to 1.32 μs. The design goals for the accumulator ring are the following:

- The lattice should be adapted to foil stripping in a first stage, but should also allow for installation of a laser stripping system. For a laser system the beam should be as small as possible in the injection region to allow for a laser to effectively focus on the beam. On the other hand, the beam should be as big as possible if a thin stripping foil is used. These considerations affects the size of the beta function in the injection region.
- There should be straight sections with room for injection magnets, RF cavities for acceleration, beam diagnostics, and collimation.
- The dispersion should be suppressed in the straight sections by enforcing a $2\pi n$ phase advance in the arcs, where n is an integer.
- The magnets should not be too tightly packed to minimize interaction of stray fields from neighbouring magnets.
- The magnets should be designed with a pole-tip fields of < 1.5 T, since this is the maximum field that normal-conducting magnet can reach [14]. Super-conducting magnets can reach higher magnetic fields, but are substantially more expensive to construct.

- The beam chamber size, as defined in chapter 2 must be big enough to fit the beam inside, but small enough fit inside the magnet aperture.

4.2 LATTICE ELEMENTS

In chapter 2, the beam transfer through an accelerator was described using an analytical solution to Hill's equation. However, by using the periodicity of the machine and the fact that the restoring force is piecewise constant, a much simpler expression can be used. In this notation, the beam coordinates (x, x') (position and angle of trajectory) at any point can be calculated from a previous point (x_0, x_0') by using the linear transfer matrix [14]

$$\begin{pmatrix} x \\ x' \end{pmatrix} = \begin{pmatrix} C(s) & S(s) \\ C'(s) & S'(s) \end{pmatrix} \begin{pmatrix} x_0 \\ x_0' \end{pmatrix} = m \begin{pmatrix} x_0 \\ x_0' \end{pmatrix}.$$

The parameters $C(s)$, $S(s)$, $C'(s)$ and $S'(s)$ depend on the type of magnet at the location s. For three elements m_1, m_2, m_3, the coordinates simply transforms as

$$\begin{pmatrix} x \\ x' \end{pmatrix} = m_3 m_2 m_1 \begin{pmatrix} x_0 \\ x_0' \end{pmatrix},$$

where the m_i are linear transfer matrices. For a full turn, all the elements are multiplied together and the final transfer matrix fulfill

$$M = \begin{pmatrix} \cos\mu + \alpha \sin\mu & \beta \sin\mu \\ -\gamma \sin\mu & \cos\mu - \alpha \sin\mu \end{pmatrix},$$

where γ and α are defined in terms of the β-function, described in chapter 2:

$$\alpha = -\frac{\beta'}{2}$$
$$\gamma = \frac{1 + \alpha^2}{\beta}.$$

In order for the beam to be stable, the magnitude of the trace of the one-turn transfer matrix must be smaller than 2. This imposes the condition [32]

$$|\cos\mu| < 1. \tag{1}$$

In other words, the phase must be real.

Drift section

In a drift section, the beam is not focused in the transversal plane and the transfer matrix is given by [14]

$$\begin{pmatrix} x \\ x' \end{pmatrix} = \begin{pmatrix} 1 & L \\ 0 & 1 \end{pmatrix} \begin{pmatrix} x_0 \\ x'_0 \end{pmatrix}.$$

Dipole magnet

Dipole magnets are used to bend the beam in the horizontal plane. The strength of the dipole magnetic field is related to the bending radius and the particle momentum through the equation [12]:

$$B\rho = \frac{p}{0.29979} \frac{GeV}{c}. \tag{2}$$

The dipole transfer matrix is approximately the same as for a drift space.

Quadrupole magnet

A quadrupole magnet focuses in the beam in one transverse direction and focuses in the other. Here, a focusing (defocusing) quadrupole is defined as the quadrupole that focuses (defocuses) in the x-direction and defocuses (focuses) in the y direction. The strength of a quadrupole is given by

$$k = \frac{1}{B\rho} \frac{dB_z}{dx}, \tag{3}$$

where k is the quadrupole strength, B the magnetic field, ρ the bending radius, and dB_z/dx the magnetic field gradient. The transfer matrix of a focusing quadrupole is given by

$$\begin{pmatrix} x \\ x' \end{pmatrix} = \begin{pmatrix} \cos\sqrt{K}l & \frac{1}{\sqrt{K}} \sin\sqrt{K}l \\ -\sqrt{K}\sin\sqrt{K}l & \cos\sqrt{K}l \end{pmatrix} \begin{pmatrix} x_0 \\ x'_0 \end{pmatrix}.$$

To obtain the transfer matrix for a defocusing quadrupole, simply change the $-$ in the second row to a $+$. It is often convenient in calculations to consider a zero-length quadrupole, that is, a quadrupole with the same focusing strength but with $l \to 0$. The rest of the space have to be replaced with a drift space of the same length as the original quadrupole. The transfer matrix of a thin focusing quadrupole is

$$\begin{pmatrix} x \\ x' \end{pmatrix} = \begin{pmatrix} 1 & 0 \\ -1/f & 1 \end{pmatrix} \begin{pmatrix} x_0 \\ x'_0 \end{pmatrix}.$$

FODO cell

The FODO cell is the most commonly used in accelerators. It consists of a focusing quadrupole (F), a drift space (O), a defocusing quadrupole (D), and another drift space (O). The drift spaces may contain dipole magnets to steer the beam. A FODO cell with dipole magnets between the quadrupoles is called an arc cell.

The FODO cell is useful because it is a very stable and reliable cell type, which makes it straightforward to use. It allows for low quadrupole magnet gradients, small variations in the lattice functions, and is easibly tunable. A drawback is that it does not allow much free space for insertion devices and instrumentation [33].

Doublet cell

A doublet cell consists of a focusing quadrupole, a defocusing quadrupole, and a drift space. The drift space is longer than in a FODO cell and is thus used where extra space is required, eg. for an insertion device.

4.3 MATCHING USING MAD-X

In the computer program MAD-X (Methodical Accelerator Design), the lattice is designed through an input file where the physical properties of each element are defined, as well as its position in the machine. A quadrupole element, for example, can be introduced like this:

```
QF: QUADRUPOLE,L=1.5,K1=0.001,THICK=1;
```

Where L is the physical length, K1 is the quadrupole strength and THICK defines the element as either thick (THICK= 1) or thin (THICK= 0). Often, the optimal strength of the quadrupole required for a stable solution is not known beforehand. It is then necessary to try a range of different values. In MADX, this is done in the environment

```
MATCH
```

The matching is done by fixing a value over a segment, such as the phase advance, or the maximum β function (the amplitude envelope) as a constraint. Then the parameter to be matched is given, with an interval of the minimum and maximum values. MADX then tries to find the parameter value that fits the constraint. This has to be iterated around the accelerator several times to find the optimal value for each parameter.

4.4 SIMILAR ACCUMULATORS

The accumulator ring for the ESSnuSB is unprecedented in that has ten times higher intensity than the previous most intensive machine, the Spallation Neutrino Source (SNS). In table 1 a comparison with similar machines is presented.

MACHINE	LENGTH	INTENSITY	ENERGY
SNS [34]	248 m	1×10^{14}	1 GeV
ISIS [35]	163 m	3×10^{13}	800 MeV
SPL [25]	318 m	1×10^{14}	5 GeV
ESSnuSB [8]	376 m	2.8×10^{14}	2 GeV

Table 1: Comparison of similar accumulator rings

Below are discussed two machines that in many way matches the requirements of the ESS accumulator: the first is the "SPL-accumulator" or Superconducting Proton Linac, under design at CERN. The second lattice was designed for SNS and it is currently in operation at Oak Ridge National Laboratory, United States.

4.4.1 *SPL-based accumulator*

The SPL accumulator consists of two straight sections and two arcs, a design refered to as ”racetrack”. It is isochronous, meaning that increasing the energy does not decrease the revolution time, since the increased velocity and increase in orbital length exactly cancel. This means that the particles will remain bunched and will not spread in the longitudinal direction [36].

4.4.2 *SNS accumulator*

The SNS lattice consists of four arcs, each consisting of four arc cells (focusing quadrupole, dipole, defocusing quadrupole, dipole) for focusing and dipoles for bending, and four straight sections made of two doublet cells each (focusing quadrupole, defocusing quadrupole, drift space), giving a lattice with a four-fold symmetry. Dispersion suppression in the lattice is achieved by imposing a 90 degrees phase advance in each arc cell, for a total of 360 degrees in each bending arc [16]. The doublets allow long sections of low-beta values (meaning small beam size), which is necessary for injection into the accumulator.

PARAMETER	VALUE	UNIT
Circumference	318	m
Injection energy	5	GeV/c^2
Particle momentum	5.86	GeV/c
Number of dipoles	50	
Dipole strength	1.6	T
Dipole length	1.6	m
Number of FODO cells	24	
Frequency	50	Hz
Number of protons	10^{14}	
Beam power	4	MW
Bending magnet length	80	m

Table 2: Parameters in the SPL-based accumulator [25]

PARAMETER	VALUE	UNIT
Circumference	248	m
Injection energy	1	GeV
Beam power	2	MW
Number of protons	$2.08 \cdot 10^{14}$	
Particle momentum	1.7	GeV
Bending radius	7.304	m
Dipole strength	0.776	T
Revolution time	0.84	μ s
Number of FODO cells	16	
Length of one FODO cell	8	m
Repetition rate	60	Hz
RMS emittance	40	π mm mrad

Table 3: Parameters in the SNS accumulator [33]

4.5 ESSNUSB ACCUMULATOR LATTICE DESIGN

A first design sketch of the ESSnuSB accumulator ring lattice is based on the SNS accumulator. This is motivated by the fact that it has similar intensity, energy, and length, and that it also uses foil stripping of H^-. This way, the ESSnuSB could potentially benefit from upgrades of the SNS accumulator since they could also be applied to the ESSnuSB accumulator. One example is installing a laser stripping system

[37]. The SNS lattice file was provided by [38], but it was written in an older version of MAD so a translation into the new format MAD-X was required. The matching sections was rewritten and each lattice element was redefined using the new syntax.

Afterwards, the lattice was upgraded to work with a 2 GeV beam. The initial quadrupole strengths was increased and the maximum β was allowed to increase up to a maximum of 50 m to allow for a stable solution. A longer lattice was required to keep the magnetic field strengths low, so the lattice was expanded to 376 m by doubling the arc length and keeping the length of the straight sections. This was done by inserting 4 extra arc cells in each bending arc, for a total of 8 arc cells in each arc. The phase advance per arc cell was held constant, so that the total phase advance in one arc is $2 \times 2\pi$, which is required for dispersion suppression (see section 2.1.2). The tune was also increased to 11.23 horizontally and 11.20 vertically, which is far from a strong resonance but does cross some weak resonance lines.

The beam dynamics in the accumulator was then simulated using MAD-X. The beam kinetic energy and type of particle is given as input. The linear transfer matrices for each element in the ring are multiplied in the program and the resulting beam optics parameters β, α, γ and the dispersion function D_y are plotted.

PARAMETER	VALUE	UNIT
Circumference	376	m
Injection energy	2	GeV
Beam power	5	MW
Number of protons	$1.1 \cdot 10^{15}$	
Particle momentum	2.78	GeV/c
Number of dipoles	64	
Number of quadrupoles	84	
Bending radius	14.6	m
Dipole field	0.635	T
Revolution time	1.32	μ s
Number of FODO cells	48	
Length of one FODO cell	8	m
Repetition rate	70	Hz
RMS emittance (95%)	37.5	π mm mrad

Table 4: Parameters in the ESSnuSB accumulator [8]

4.6 RESULTS AND CONCLUSIONS

A first accumulator lattice for ESSnuSB was designed and the resulting beam optics functions are plotted in figure 4.3 (beta functions) and figure 4.4 (dispersion function). The ring as seen from above is plotted in figure 4.2. By basing the design on the SNS accumulator ring, technology transfer between the two projects is enabled which can bring the costs down. The injection region is preserved in it's original design to allow for future installation of a laser stripping system which is currently being studied at SNS. The maximum dipole field strength of 0.635 is below the limit of 1.5 T so that normal-conducting magnets can be used. The lattice needs to be further developed in future studies. The maximum aperture size must be determined to limit the maximum β function and acceptance. The lattice should be better optimized to match other constraints such as quadrupole field strength, and if the ESS linac is upgraded in energy, care must be taken to ensure that the lattice will work with the new parameters. A substantial increase in energy could make it impossible to match the same lattice within acceptable field strenghts. The injection section, with a magnet bump system, need to be designed to work with both foil stripping and laser stripping. Finally, other elements should be designed and added to the lattice; RF cavities for acceleration, beam collimation, and beam diagnostics.

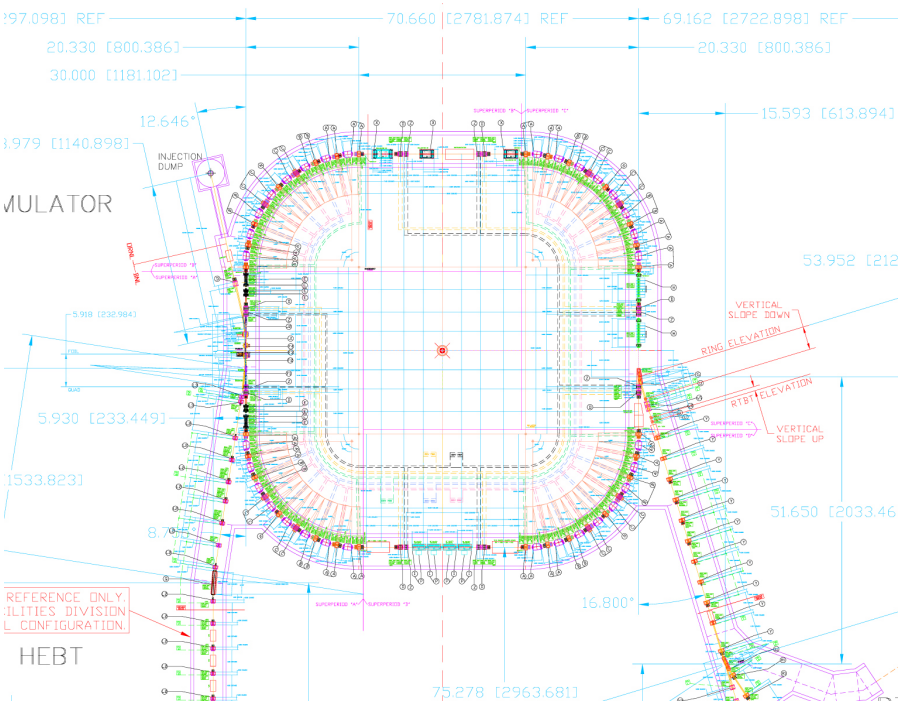

Figure 4.1: The SNS accumulator ring

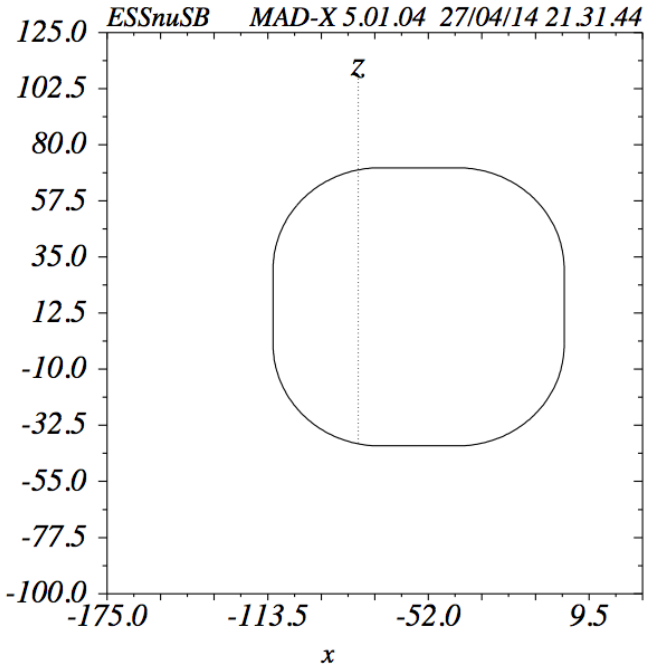

Figure 4.2: The ESSnuSB accumulator ring with four arcs and four straight section with room for insertion, RF, collimation, and beam instrumentation. The total circumference is 376 m.

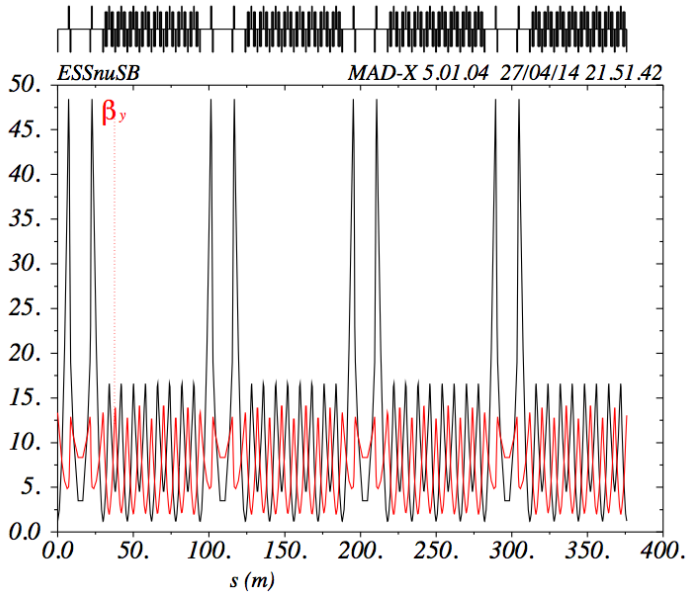

Figure 4.3: The ESSnuSB accumulator beta functions (red: vertical, black: horizontal). The straight sections have 15 m long low β drift spaces.

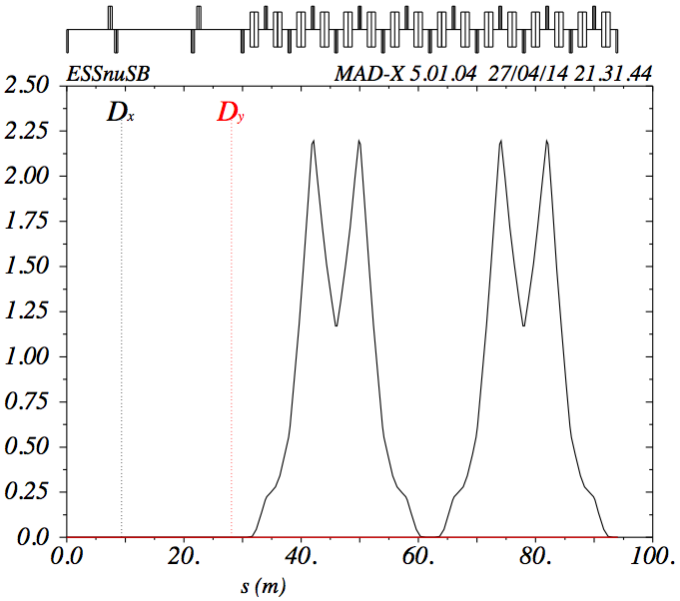

Figure 4.4: Dispersion in a superperiod, consisting of one straight section and one arc. Dispersion is suppressed by forcing a 4π phase advance in the arc, or $\pi/4$ per arc cell.

5

PROJECT CONCLUSIONS

The ESSnuSB is a project to detect and measure neutrino CP-violation using the ESS linear accelerator. Four 0.7 ms long H^-pulses containing 2×10^{14} ions will be accelerated to 2 GeV between each proton pulse for neutron spallation. The H^-will then be deflected and led towards a target station, where pions are produced. The pions are focused towards the detectors by a pulsed magnet with a peak current length of about 5 μs. They are let to decay in a decay tunnel, and the produced neutrinos continue in the same direction. To shorten the 0.7 ms long H^-pulses to less than 5 μs, an accumulator ring will be placed between the linac and the target station. The aim of the project was to study two issues related to the high intensity of the beam in the accumulator; defocusing forces due to the space-charge of the beam, and foil stripping of the H^-during injection into the ring. A third aim was to design an accumulator lattice using the design parameters of the ESSnuSB.

The space charge tune shift in the accumulator for the ESSnuSB parameters was evaluated. By modeling the beam intensity as a gaussian distribution, it was found to be 0.0968 which is well below the maximum acceptable space charge tune shift of 0.2. This model can be further improved by including the effects of a bunched beam. To ensure that foil stripping is a feasible method to remove the electrons from the H^-during injection, the maximum temperature induced on the carbon stripping foil by the incoming beam was simulated. The results showed that the temperature on the foil did not rise above the threshold temperature (2500 K), so that foil stripping can be used provided that the beam cross section on the foil can be made big enough. Whilst the values obtained are in line with current studies, the model can be further improved by including the heating of the circulating beam and the 3D-geometry of the foil. Finally, a cost-effective accumulator lattice was designed by upgrading the Spallation Neutron Source accumulator lattice to a higher energy. This allows for technology transfer between the two projects. The lattice can be further improved by designing a magnet bump system for injection and by optimising the matching of the magnet strengths.

BIBLIOGRAPHY

[1] Griffiths D. Introduction to Elementary Particles. 6th ed. Wiley; 2008.

[2] An FP, Bai JZ, Balantekin AB, Band HR, Beavis D, Beriguete W, et al. Observation of electron-antineutrino disappearance at Daya Bay. Phys Rev Lett. 2012;(108):171803.

[3] Abgrall N, Aihara H, Akiri T, Albert JB, Andreopoulos C, Aoki S, et al. Evidence of Electron Neutrino Appearance in a Muon Neutrino Beam. Phys Rev D. 2013;(88):032002.

[4] Beringer J. Neutrino mass, mixing, and oscillations. Phys Rev D. 2012;(86):010001.

[5] Coloma P, Fernandez-Martinez E. Optimization of neutrino oscillation facilities for large θ_{13}. Journal of High Energy Physics. 2012 April;(89).

[6] Peggs S. ESS Technical Design Report. ESS; 2013.

[7] Wildner E. Private communication; 2014.

[8] Baussan E, Blennow M, Bogomilov M, Bouquerel E, Cederkall J, Christiansen P, et al.. A Very Intense Neutrino Super Beam Experiment for Leptonic CP Violation Discovery based on the European Spallation Source Linac: A Snowmass 2013 White Paper; 2013.

[9] Lombardi AM. The Radio Frequency Quadrupole (RFQ); 2005. CERN Accelerator School (CAS) Lecture Notes.

[10] Coughlan G, Dodd E, Gripaios B. The Ideas of Particle Physics. Cambridge University Press; 1991.

[11] Wildner E. ESSnuSB Compressor Ring; 2014. ESSnuSB Open Meeting CERN 2014.

[12] Wilson E. An Introduction to Particle Accelerators. Oxford University Press; 2001.

[13] Wille K. The Physics of Particle Accelerators. Oxford University Press; 2000.

[14] Wiedemann H. Particle Accelerator Physics. Springer; 2007.

[15] Tomás R. From Farey sequences to resonance diagrams. Phys Rev ST Accel Beams. 2014 January;(17):014001.

[16] Henderson S, Holmes J, Zhang Y. Off-Momentum Effects and Longitudinal Dynamics in Rings; 2009 [cited April 27 2014]. Available from: http://uspas.fnal.gov/materials/09VU/VU_Fund.shtml. USPAS Lecture notes, Lecture 8.

[17] Schindl K. Space Charge; 2006. CERN Accelerator School (CAS) Lecture Notes.

[18] Wildner E. ESSnuSB Accumulation Ring; 2014. ESSnuSB Open Meeting Lund 2014.

[19] Bartmann W. Laser Stripping for H- Injection; 2014. ATS Seminar.

[20] Assmann R, Leemans W, Mitsuru U, Hoffmann I. High Power Laser Technology for Accelerators: A joint International Committee on Future Accelerators (ICFA) and International Committee on Ultrahigh Intensity Lasers (ICUIL) whitepaper; 2000.

[21] Lebedev SG, Lebedev AS. Calculation of The Lifetimes of Thin Stripper Targets Under Bombardment of Intense Pulsed Ions. Phys Rev ST Accel Beams. 2008 February;(11):020401.

[22] Sugai I. Lifetime measurement of HBC-foil and nanocrystalline diamond foil by using KEK-650 KEV high intensity H-DC beam. In: Proceedings of Hadron Beam; 2008. p. 300.

[23] Gulley MS. Measurement of H-, Ho, and H+ yields produced by foil stripping of 800-MeV H- ions. Physical Review A. 1996 May;(53):3201.

[24] Liaw CJ, Lee YY, Tuozzolo J. Life time of carbon stripping foils for the spallation neutron source. In: Proceedings of the 2001 Particle Accelerator Conference. BNL; 2001. p. 1538–1540.

[25] Aiba M. Feasibility Study of Accumulator and Compressor for the 6-bunches SPL based Proton Driver. CERN; 2008.

[26] NIST. Pstar; 2013 [cited December 2013]. Available from: http://physics.nist.gov/PhysRefData/Star/Text/PSTAR.html.

[27] NIST. Estar; 2014 [cited January 2014]. Available from: http://physics.nist.gov/PhysRefData/Star/Text/ESTAR.html.

[28] Liaw CJ, Lee YY, Alessi J, Tuozzolo J. Calculation of the maximum temperature on the carbon stripping foil of the spallation neutron source. In: Proceedings of the 1999 Particle Accelerator Conference. BNL; 1999. p. 3300–3302.

[29] Liaw CJ, Lee YY, Alessi J, Tuozzolo J. Maximum Temperature on the Carbon Stripping Foil In the Spallation Neutron Source. Brookhaven National Laboratory; 1998.

[30] Martini M. Private communication; 2014.

[31] Schönauer H. Private communication; 2014.

[32] Germain P. Introduction aux accélérateurs de particules. CERN; 1989.

[33] Wei J. Low-loss design for the high-intensity accumulator ring of the Spallation Neutron Source. Phys Rev ST Accel Beams. 2000 August;(3):080101.

[34] Weng WT. Accumulator ring design for the NSNS project. In: Proceeding of: Particle Accelerator Conference. Brookhaven National Laboratory; 1997. p. 970–972.

[35] Warsop CM. Studies of space charge loss mechanisms on the ISIS synchrotron. In: Proceedings of the 2007 Particle Accelerator Conference; 2007. p. 1652 – 1654.

[36] Aiba M. Revisit to the SPL accumulator and compressor design for NF (and SB); 2012. ABP forum.

[37] Gorlov T, Danilova V, Aleksandrov A, Liu Y. Status of laser stripping at the SNS. In: Proceedings of 2011 Particle Accelerator Conference; 2011. p. 2035–2037.

[38] Papaphilippou Y. Private communication; 2014.

ACKNOWLEDGMENTS

Many thanks to Elena and Tord for organising this project. Thanks also to Horst, Michel, Yannis, and many others at the CERN Beams Department for their help and discussions.